ACSNANO

www.acsnano.org

ARTICLE

COVID-19 Spike Protein Induced Phononic Modification in Antibody-Coupled Graphene for Viral Detection Application

Ngoc Hoang Lan Nguyen, Sungjoon Kim, Garrett Lindemann, and Vikas Berry*

Cite This: *ACS Nano* 2021, 15, 11743–11752

Read Online

ACCESS | Metrics & More | Article Recommendations | Supporting Information

ABSTRACT: With an incubation time of about 5 days, early diagnosis of severe acute respiratory syndrome coronavirus 2 (SARS-CoV-2) is critical to control the spread of the coronavirus disease 2019 (COVID-19) that killed more than 3 million people in its first 1.5 years. Here, we report on the modification of the dopant density and the phononic energy of antibody-coupled graphene when it interfaces with SARS-CoV-2 spike protein. This graphene chemeo-phononic system was able to detect SARS-CoV-2 spike protein at the limit of detection of ∼3.75 and ∼1 fg/mL in artificial saliva and phosphate-buffered saline, respectively. It also exhibited selectivity over proteins in saliva and MERS-CoV spike protein. Since the change in graphene phononics is monitored instead of the phononic signature of the analyte, this optical platform can be replicated for other COVID variants and specific-binding-based biodetection applications.

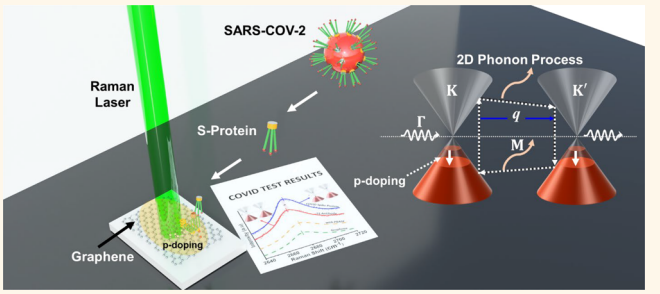

KEYWORDS: *COVID-19, SARS-CoV-2 spike protein, graphene, phononic detection, Raman spectroscopy*

In December 2019, a highly infectious coronavirus disease 2019 (COVID-19) was first reported in Wuhan, China.[1,2] In March 2020, the World Health Organization (WHO) classified the COVID-19 as a pandemic, which by May 2021 had taken more than 3.5 million lives and infected more than 160 million people.[3] The COVID-19 virus belongs to the beta-coronavirus family including SARS-CoV (severe acute respiratory syndrome coronavirus) and MERS-CoV (Middle East respiratory syndrome coronavirus). COVID-19 is caused by the SARS-CoV-2 virus, which is composed of a single-stranded RNA genome enclosed in a membrane forming a spherical structure approximately 125 nm in diameter. There are four major proteins encoded by the COVID-19 genome: the spike (S) protein, nucleocapsid (N) protein, membrane (M) protein, and the envelope (E) protein.[4] Structurally, the spike protein is composed of a transmembrane anchor, a short intracellular tail, and a large ectodomain, which includes the receptor-binding domain. Functionally, the spike protein is responsible for binding with the host cell receptors (such as angiotensin converting enzyme 2 (ACE-2)[5]), which mediates the entry of the virus into the target cells. Due to its functional importance and its location on the outer shell of the COVID-19, this work is focused on the effect of the interfacing of the spike (S) protein on the phononics of graphene (functionalized with antibody).

Since a large population of people that contract the coronavirus are asymptomatic and most others develop symptoms in 3 to 5 days (due to the long viral incubation time), fast diagnosis is critical in controlling the pandemic. By April 2021, the FDA had approved over 240 diagnostic tests for COVID-19 (through emergency use authorization), of which ∼90% were based on RT-PCR amplification and detection of viral RNA. Other COVID-19 sensors are based on protein (N protein found in blood and saliva), antibody (mostly IgM and IgG), and whole viral particle detection via ELISA or optical and electrical transducers. Being an established technique, RT-PCR (including loop-mediated isothermal amplification (LAMP)), offers high-throughput capacity, high sensitivity, and specificity, as well as detectability of active cases, which makes it especially useful in clinical decision making. However, this method has some limitations, which include the following: 1. Several reagents and procedural

Received: March 24, 2021
Accepted: June 10, 2021
Published: June 15, 2021

https://doi.org/10.1021/acsnano.1c02549
ACS Nano 2021, 15, 11743–11752

steps (purification, transcription, amplification, and detection) are required, which increases the time from acquisition of sample to reporting of the outcome. Thus, depending on the test and logistics, the time can range from minutes, to days, to weeks. 2. High volume testing equipment are usually located in large laboratories that are commercial, clinical, or at a hospital complex that have several CLIA certifications, including one for high-complexity tests. 3. The medical criteria are subjective in nature—fever, cough, shortness of breath—as well as the difficulty of patients knowing if they have been in contact with a person actively shedding COVID-19 virus particles.[6−8] These necessitate the development of a virus detection platform that is simple and capable of providing quick results, while still being reliable. For non-nucleotide detection, there is a study on electrical response from a transistor that can detect COVID proteins.[9] However, the fabrication of such devices necessitates the incorporation of photolithography and deposition processes, which increase the cost of individual sensors. Further, the electronic flow through such systems can interfere with the analyte or cause electrochemical side reactions on the sensor surface.[10] Devices based on the surface plasmon resonance (SPR) of two-dimensional gold nanoislands and nanoparticles have also been investigated.[11,12] SPR is the coherent oscillation of surface conduction electrons driven by photons and is sensitive to surface coupling events such as molecular binding and changes in refractive index. Another method uses chemiluminescence for IgG and IgM detection, where labeled protein is interacted with the antibody in saliva, and the presence of the antibody is detected *via* a change in luminescence (in some cases magnetic beads are attached to concentrate the sample).[13−15] A modified fluorescence detection method is lateral flow immunoassay, where the antibody (anti-IgM or IgG)/protein or rNA/DNA interaction is detected in a hand-held device.[16] The results from the detection system presented in this work are compared with other detection techniques in Table 2.

Table 1. Change in Fermi Level and Doping with SARS-CoV-2 Spike Protein Concentrations

Concentration	2D peak position (cm^{-1})	ΔE_f (meV)	$\Delta p \left(10^{11}\frac{\text{dopant}}{cm^2}\right)$
antibody	2681.79		
1 pg/mL	2682.62	−26.9	9.7
100 pg/mL	2683.34	−23.4	9.1
10 ng/mL	2683.77	−14.2	5.7
1 μg/mL	2685.96	−83.5	39.4
10 μg/mL	2686.17	−10.6	5.6

Here, we show the change in phononic energies of antibody-coupled graphene with the selective binding to the COVID-19 spike protein for its detection (Figure 1). Among the available phononic modes (D, D′, G, 2D, and 2D′),[17] graphene's properties are predominantly represented by the following three phonon vibrational modes: D-band peak (intervalley phonon) near 1350 cm^{-1}, G-band peak (E_{2g}, primary in-plane vibrational mode) around 1580 cm^{-1}, and 2D-band peak (second-order overtone of a different in-plane vibrational mode) at about 2670 cm^{-1} (peak positions are for a 532 nm incident laser). Since graphene has a monatomic thickness, these peaks are highly sensitive to its structural, electronic, and interfacial properties.[18] In particular, Raman peak positions correlate strongly with its doping level represented by the concentration of charge carriers in graphene (dopants/cm^2).[19]

While the 2D peak position increases with p-doping and decreases with n-doping (for both n- and p-type graphene), the G peak position increases with n-doping for n-type graphene and with p-doping for p-type graphene.[17,19] This implies that the G band can provide information only on the change in carrier density, while the 2D band can provide the carrier density and the polarity of doping. In addition, the G band (Raman-active E_{2g} Γ phonon mode) exhibits a Kohn anomaly.[20−23] With heavy doping, the adiabatic Born−Oppenheimer approximation, which is valid in many solid-state systems, breaks down, causing phononic vibration for the G peak to stiffen and eventually results in the saturation of the G peak shift.[19,24−26] However, since the nonadiabatic effect does not influence the 2D phonon, the 2D band position is not limited by high carrier concentration. Therefore, in this work, we study the 2D peak position to calculate the doping concentration and polarity for the identification of the COVID-19 spike protein. Unlike previous work on detecting glioblastoma multiforme cells[27] and amyotrophic lateral sclerosis,[28] this work includes specific binding agents on graphene for improved selectivity. It is important to note that this detection platform can be employed for other COVID variants as well as whole viral particle detection and that this is a direct measurement of a viral antigen attachment.

While Raman spectroscopy has been employed for identifying "fingerprint" peaks of analytes,[29,30] here we show an analyte-specific Raman transducer that undergoes a phononic change with attachment of a targeted molecule. A robust Raman transducer platform should have sensitive phononic properties that are coupled with its interfacial properties. Graphene satisfies this requirement, owing to its two-dimensional confinement of sp^2-hybridized carbon atoms with an overlapping electron cloud, strong electron−phonon coupling, and a high quantum capacitance. Further, graphene's surface chemistry can be readily modified to attach analyte-binding molecules. These properties allow graphene to be phononically sensitive to small changes in doping from an analyte attachment.

Table 2. Comparison between Current Work and Other Protein-Based Biosensors

method	target analyte	sample type reported	LOD	advantages	limitations
phononic sensor (this work)	antigen/ antibody	artificial saliva, buffer	1 fg/mL 25 aM	potential for real-time detection, low fabrication cost devices, quick analysis	spectrometer is relatively expensive
FET sensor[9]		respiratory, buffer	1 fg/mL	real-time detection, quick analysis	high fabrication and testing cost
plasmonics[11]	virus mRNA	respiratory, buffer	0.2 pM	real-time detection, quick analysis	relatively low accuracy, spectrometer is relatively expensive, high fabrication cost

https://doi.org/10.1021/acsnano.1c02549
ACS Nano 2021, 15, 11743−11752

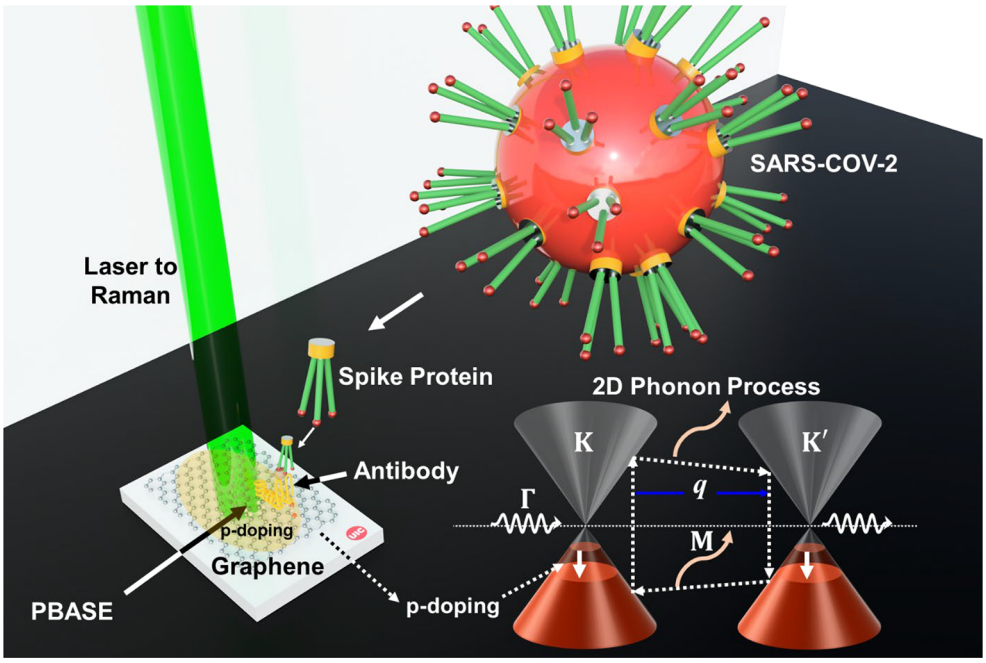

Figure 1. Schematic depicting the mechanism of the graphene-phononic transducer, where COVID-19 spike protein's attachment with antibody on graphene changes the energy levels within graphene's Dirac cones, thus modifying its 2D mode's phononic energy. Also shown is the graphical representation of the Dirac cones with wave vector *q*, Brillouin zone center Γ, M points in the middle of the hexagonal sides, and K and K′ points representing the corners of the hexagons. The schematic is not to scale and is not an accurate representation of the components.

For the process mechanism, consider a molecule coming in close proximity to graphene. The molecule can modify graphene's carrier concentration *via* two prominent routes: (a) charge transfer due to the relative positions of the Fermi level of graphene and the highest occupied molecular orbital (HOMO) (for electron donors) or lowest unoccupied molecular orbital (LUMO) (for electron acceptors) levels of the interfacing molecule, and (b) dipole moment gating, which is amplified by the large quantum capacitance of graphene.[31] This doping modifies the electronic band, which renormalizes the 2D phonon's resonance conditions (Figure 1). When the electronic band is pushed away from the Dirac point, the absolute value of electron energy increases, leading to the decrease of the excited quasiparticle's lifetime and phonon momentum.[32] This process causes a change in the 2D mode Raman shift and its scattering phononic energies, correspondingly. It is important to note that high-quality graphene is critical for this process, because defects (lattice disorders and oxy groups) lead to the combination of intervalley phonon and defect scattering forming the D peak, thus significantly suppressing the two phonon scattering of the 2D peak. Moreover, the defect sites on the graphene lattice can attract nonspecific binding, which would affect the selectivity of the biosensors.

The sensing mechanism of this graphene chemeo-phononics lends simplicity to the final device construct: (a) No electrical connections are required, eliminating the need for photo- or electron-lithographic techniques;[10] (b) direct measurements; (c) no electrochemical side-reactions; and (d) requires fewer reagents. The main challenge of the technique is the relative high cost of the Raman spectrometer required for detection and the data analysis, which can be mitigated for high-volume operations.

In this work, graphene is functionalized with a CoV-2 spike RBD antibody (amino acid sequence from Arg 319 to Phe 541; polyclonal rabbit IgG, 40592-T62; Sino Biological, Inc., China) that binds specifically to the CoV-2 spike RBD protein (amino acid sequence from Arg 319 to Phe 541; ab273065; Abcam, Inc., USA) (more information is provided in the Supporting Information). The vicinity of the spike protein bound to the antibody leads to a p-doping of the p-type graphene, in turn causing a blue-shift in the 2D peak. This graphene phononic device exhibits a limit of detection (LOD) of ∼1 and 3.75 fg/mL of SARS-CoV-2 antigen spike protein in PBS and in artificial saliva, respectively. Moreover, the sensor showed selectivity due to the precision of antibody−antigen binding. It could distinguish SARS-CoV-2 spike protein from a complex mixture of other proteins and enzymes in artificial saliva as well as another member in the betacorona virus family: MERS-CoV spike protein.

RESULTS AND DISCUSSION

The study was carried out on graphene sheets produced *via* chemical vapor deposition (CVD) on copper foil and transferred on a Si/SiO_2 300 nm wafer.[33] Due to the oxy and hydroxy groups on the silicon oxide surface, the graphene-on-SiO_2 becomes a p-type semimetal.[34] To immobilize the antibody on graphene, it is first interfaced with a 1-pyrenebutyric acid *N*-hydroxysuccinimide ester (PBASE) linker, which has an aromatic pyrene group that binds with graphene *via* $\pi-\pi$ interaction. Its amine-reactive group is then bound with the amino acid groups on the specific antibody of SARS-CoV-2 spike protein (Figure 1). The PBASE/graphene reaction is carried out in methanol for 1 h at room temperature. It is known that based on the HOMO and LUMO of the aromatic molecules and their electron-withdrawing or electron-donating groups, they can either p-

https://doi.org/10.1021/acsnano.1c02549
ACS Nano 2021, 15, 11743−11752

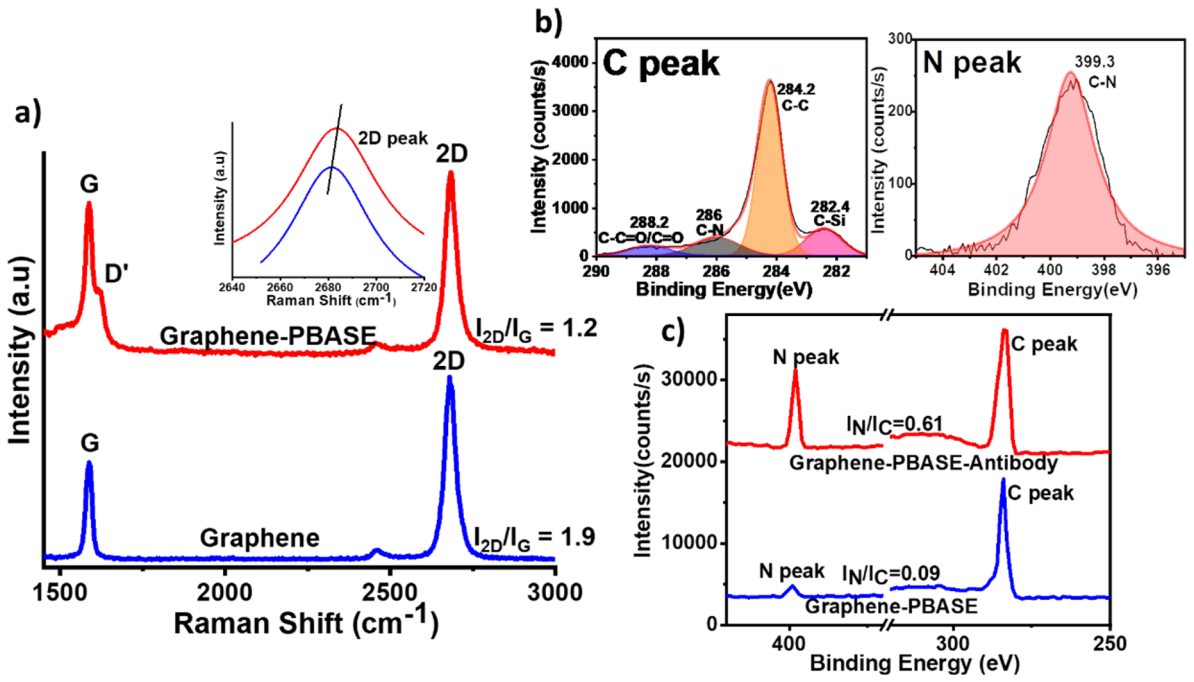

Figure 2. (a) Representative Raman spectra of the pristine graphene and PBASE-treated graphene. The inset shows an upshift of the Raman 2D band after attachment of PBASE. (b) High-resolution XPS spectra of graphene-PBASE at the C 1s peak and N 1s peak, respectively. (c) XPS survey scans of graphene-PBASE and graphene-PBASE-antibody structures.

dope or n-dope the graphenic materials, respectively.[35] Previous work has shown that the ester and nitrogen groups in PBASE are responsible for withdrawing the electrons directly from graphene to p-dope it,[35] and the work function of graphene increases by 0.5 eV after PBASE attachment,[36] indicating electrons transfer from graphene's Fermi level to the LUMO level of PBASE. Here, the electronic band is pushed further below the Dirac point, which is reflected in a blue-shift of the 2D peak position (Figure 2a, discussed next). In addition, the van der Waals force between the graphene and the pyrene backbone of the PBASE molecule ensures their tight binding and retention of the sp^2-carbon lattice construct. To confirm the attachment of PBASE on graphene, Raman spectroscopy and X-ray photoelectron spectroscopy data were collected. All Raman spectra were acquired using a confocal Raman microscope (Raman-AFM, WITec alpha 300 RA, laser wavelength of 532 nm). The laser spot size was ~721 nm with a 50× objective lens (ZEISS). Figure 2a shows a comparison between Raman spectra of pristine graphene and graphene functionalized with PBASE. In pristine graphene, the presence of two major G and 2D peaks with a very small D peak indicates the high quality of the transferred graphene with minimal defects (intensity ratio I_{2D}/I_G = 1.9 and I_D/I_G = 0.04). After the attachment of PBASE, there was an emergence of the D′ (1623 cm^{-1}) peak. The D′ peak is attributed to a resonance of the pyrene group onto the graphene surface and the high edge density. This confirms the attachment of PBASE onto the graphene. In addition, the 2D peak position was shifted to a higher frequency and the I_{2D}/I_G ratio decreases after the attachment, consistent with previous work.[9,37,38]

Figure 2b shows the high-resolution X-ray photoelectron spectroscopy (XPS, Kratos AXIS-165) spectra of PBASE-treated graphene at the C 1s peak and N 1s peak. The appearance of the core N 1s peak further confirms the presence of PBASE on graphene. In particular, the peak at a binding energy (BE) of ~399 eV is assigned to the C−N bonds.[39] The C 1s peak was deconvoluted into four components: 282.4, 284.2, 286, and 288.2 eV, corresponding to C−Si, C═C, C−N, and C═O/C−C═O bonds, respectively.[9] While the strongest peak (C═C) is attributed to graphene, the presence of oxygen-functionalized carbon C═O/C−C═O is due to the residue of poly(methyl methacrylate) (PMMA) from the graphene-transferring process. More importantly, the presence of a C−N peak in both C 1s peak and N 1s peak scans confirms the chemical attachment of PBASE on graphene.

The immobilization of SARS-CoV-2 spike antibody on PBASE-modified graphene was performed through the interaction between the antibody's amine ($-NH_2$) group and the *N*-hydroxysuccinimide ester group of PBASE. The XPS survey data from Figure 2c reveal that after antibody modification there is a significant increase in the intensity of the N 1s peak. There is also a slight increase in C 1s peak intensity; however, the ratio between N 1s:C 1s peak intensities increased 6.6 times (0.09 to 0.61) after antibody attachment. This increase in the number of nitrogen atoms is attributed to the amino acid groups of the antibodies. In addition, from the analysis of the XPS peaks of C and N, the ratio of the nitrogen and the carbon atoms added is 0.275, consistent with the composition of a typical protein,[40] confirming the attachment of the antibody (see the Supporting Information).

To investigate the performance of the graphene phononic sensor, we interfaced the SARS-CoV-2 spike protein on the graphene-PBASE-antibody structure and studied the graphene's phononic response *via* Raman spectroscopy. It is important to note that the base sensitivity of graphene is dependent on all the factors that influence the 2D peak position, which includes the local temperature,[41,42] local stresses,[43−48] defects,[49] and substrate chemistry/dielectric properties.[50,51] Therefore (unless industrial level consistency

https://doi.org/10.1021/acsnano.1c02549
ACS Nano 2021, 15, 11743−11752

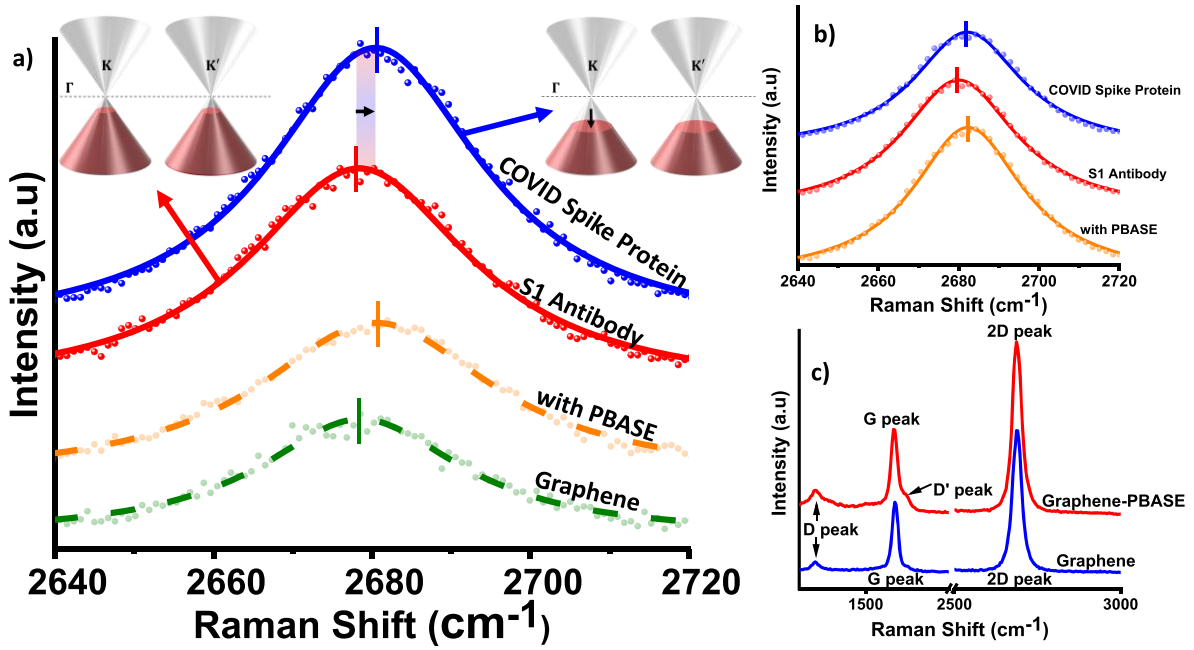

Figure 3. COVID spike protein detection via graphene phononics in (a) PBS and (b, c) artificial saliva media. The 2D Raman peak of graphene (green), PBASE-modified graphene (orange), graphene-PBASE-antibody (red), and graphene-PBASE-antibody-spike protein (blue) structures are shown. The attachment of PBASE p-dopes graphene, and the subsequent attachment of antibody n-dopes it. Further, the COVID protein attachment p-dopes the base graphene by (a) 2.07 ± 0.168 cm^{-1} for PBS and (b) 2.2 ± 0.15 cm^{-1} for artificial saliva media. (c) Raman spectra of the pristine graphene and PBASE-functionalized graphene acquired at the same location (before detection in saliva medium). The emergence of a D′ peak and the increase of D peak intensity confirm the attachment of PBASE on graphene. For (a) and (b): dots: acquired Raman data points; lines: Lorentzian fit of the 2D peak.

is achieved), each device will have its own calibration curve. The Raman spectra and areal scans were acquired at the exact same area for each of the process steps: graphene, PBASE-modified graphene, graphene-PBASE-antibody, and graphene-PBASE-antibody-spike protein structure. Here, we show a representative data scan collected to compare the doping effect after each reaction in PBS buffer (Figure 3a) and in artificial saliva medium (Figure 3b,c). In the case of the spike protein incubation in PBS buffer, initially graphene's 2D-band peak position (green) was at 2678.61 cm^{-1}. This higher value is attributed to the p-doping from the SiO_2 substrate (work function (5.0 eV) less than that of graphene). The 2D peak full-width at half maxima (FWHM) of the initial p-doped graphene is 31.1 cm^{-1}, which indicates that the graphene is single layer (good quality).[52] On the same area, PBASE π-stacking attachment showed a blue-shift of 1.89 cm^{-1} (from 2678.61 to 2680.5 cm^{-1}). As mentioned earlier, this p-doping effect is attributed to the nitrogen and ester groups on the PBASE that withdraw electrons from graphene. Next, the attachment of the spike antibody exhibited n-doping (electron injection) with the 2D peak's red-shift of 2.11 cm^{-1} (from 2680.5 to 2678.39 cm^{-1}). This is attributed to the replacement of the *N*-hydroxysuccinimide (NHS) group in PBASE with the amine group in the antibody. Because the NHS ester, which consists of two N−C═O centers, is an electron-withdrawing group,[53] the removal of the NHS group makes graphene less p-doped, which is represented by a decrease in the 2D band peak wavenumber.

Finally, upon the attachment of the spike protein (10 μg/mL in PBS buffer), there was a p-doping of graphene with a blue-shift in 2D peak position of 2.07 cm^{-1}, from 2678.39 to 2680.46 cm^{-1}. Studies have shown that the HOMO of S1 spike protein is −5.16 eV,[54] which is lower than the Fermi level of modified graphene: −4.7 eV.[36] This means that electrons will not transfer directly due to the energy level difference between the protein and graphene. Similarly, the LUMO of S1 spike protein at −2.77 eV[54,55] is higher than the Fermi level of modified graphene, indicating that electrons will not be withdrawn from graphene to the protein. Thus, we conjecture that the p-doping effect of the protein attachment is a result of induced charge carriers. When the spike protein comes in close proximity to the graphene sheet, the molecular dipoles on the protein apply an electric field (or a small gating voltage) on graphene. The polarity of the induced charge carriers is opposite the polarity of the applied voltage.[31] As the protein has a negative potential,[56] positive charge carriers were doped, leading to p-doping of graphene.

Graphene ultrasensitive doping is an outcome of high quantum capacitance, C_Q. For monolayer graphene, $C_Q = \frac{4e^2\sqrt{\pi}}{h v_F}\sqrt{n_T}$, where h is Planck's constant, $v_F \approx c/300$ is the Fermi velocity of the Dirac electron, e is the electron charge, and n_T is the total charge concentration of graphene.[57] As graphene has a large quantum capacitance (and slightly larger for CVD graphene),[58] a small potential (V) from a dipole moment can lead to high change in the electric charge (Q) on graphene (or a doping effect). Further, the 2D peak position can be correlated with the change in the Fermi level and the p-doping for p-type graphene by the following equations:[49] 2D pos. $= -2 \times 10^{-10} \times E_f^4 - 6 \times 10^{-8} \times E_f^3 + 6 \times 10^{-5} \times E_f^2 - 0.0003 \times E_f + 2676.7$, p − density $= 6 \times 10^7 \times (E_f)^2$, and the induced potential doping is estimated by $\Delta V = \frac{\Delta Q}{C_Q}$. With this, we estimate the change in Fermi level $\Delta E_f = -82.7$ meV; the change in p-doping

https://doi.org/10.1021/acsnano.1c02549
ACS Nano 2021, 15, 11743−11752

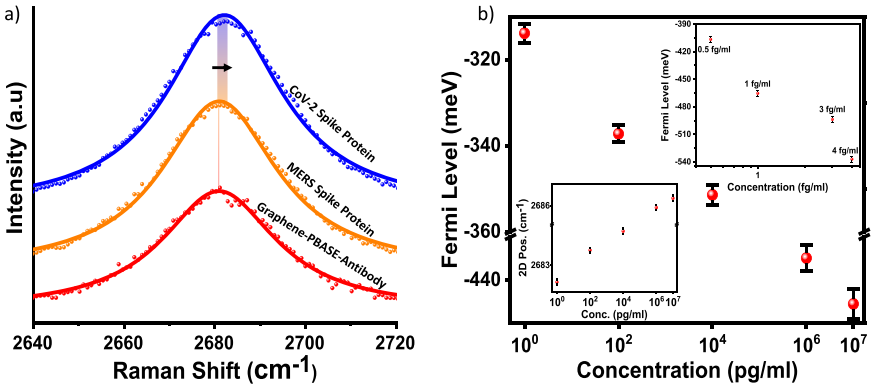

Figure 4. Selectivity and sensitivity: (a) 2D Raman peak spectra of the graphene-PBASE-antibody device (red), after interaction with MERS-CoV protein (orange) and after interaction with COVID spike protein (blue). While the interaction with MERS-CoV protein showed a negligible change in the 2D peak position, the interaction with COVID spike protein increased the 2D peak position by 1.18 ± 0.2 cm^{-1}. (b) The 2D peak position (inset (bottom, left)) and the Fermi level of graphene change with the concentration of the COVID spike protein in PBS (1 pg/mL, 100 pg/mL, 10 ng/mL, 1 μg/mL, and 10 μg/mL). The inset (top, right) shows the change in Fermi level of graphene at low concentrations (0.5, 1, 3, and 4 fg/mL) of spike protein in artificial saliva medium.

density $\Delta p = 4.1 \times 10^{11} \frac{\text{dopant}}{\text{cm}^2}$; and induced voltage $V < 12.8$ mV for spike protein attachment in PBS. In addition, the FWHM of the graphene-PBASE-antibody-protein structure increases slightly to 32.9 cm^{-1} (1.8 cm^{-1} increase from pristine graphene), showing that the graphene quality (low defect density) was maintained during all three steps (more information on the phosphate-buffered saline liquid scan is provided in the Supporting Information)

Similarly, we examine the response of the graphene phononic sensor to SARS-CoV-2 spike protein in artificial saliva in an attempt to simulate clinical samples. The saliva contains a complex mixture of proteins (*i.e.*, mucin), enzymes (*i.e.*, amylase), and minerals with a pH similar to human saliva. A similar doping and phononic response was observed. The first step of PBASE functionalization on graphene is verified by the presence of a D′ peak at around 1620 cm^{-1} and the increase in the D peak intensity as shown in Figure 3c. On that same location, the attachment of antibody shifts the 2D peak position of graphene by 2.39 cm^{-1} (from 2682.35 cm^{-1} to 2679.96 cm^{-1}) (n-doping). Spike protein in artificial saliva solution at 10 μg/mL was used for detection on the graphene-PBASE-antibody device. As expected, the 2D peak position blue-shifts by 2.2 cm^{-1} (from 2679.96 cm^{-1} to 2682.16 cm^{-1}) upon the attachment of the spike protein (p-doping) (as shown in Figure 3b). Since each viral particle's surface has approximately 100 trimers/μm^2 of S-protein,[59] we can expect a strong response from the viral particle attachment.

To investigate the selectivity of the phononic device, the antibody-coupled graphene was incubated with artificial saliva as a control experiment. Twenty locations on the sample were tested and showed practically no response after saliva incubation. Specifically, the average 2D peak position of the graphene-PBASE-antibody structure was 2677.8 ± 0.13 cm^{-1}, and this value was 2677.42 ± 0.97 cm^{-1} after saliva incubation. The average change in the peak position was −0.38 cm^{-1}, which is within the error margin and is in the opposite direction of the change expected for COVID-19 protein. This indicates that other proteins in saliva do not attach on the antibody functionalized on graphene, and the device shows minimal nonspecific binding.

In addition to a selectivity test of other complex components in saliva, MERS-CoV spike protein was used to further confirm the specificity of the antibody. As before, the same location of graphene was scanned for each of the steps in this experiment. Similar to other tests, PBASE interaction showed p-doping, and the SARS-CoV-2 spike antibody attachment showed n-doping. The graphene-PBASE-antibody device (red line in Figure 4a) was exposed to MERS-CoV spike protein (10 μg/mL) to test the device-selectivity. The Raman 2D peak shows practically no shift (0.06 cm^{-1} increase within the error range of ±0.24 cm^{-1}), which indicates no change in graphene's energy band. This result is attributed to the lack of interaction between the SARS-CoV-2 antibody and the MERS-CoV spike protein. The same device was then interfaced with the SARS-CoV-2 protein, and a p-doping was observed as expected (blue line in Figure 4a). The 2D band peak position upshifts 1.18 cm^{-1} from 2680.91 cm^{-1} (the antibody) to 2682.09 cm^{-1} (SARS-CoV-2 spike protein). From the 2D peak position, the changes in the Fermi and doping levels are estimated: $\Delta E_f = -38.9$ meV; $\Delta p = 9.1 \times 10^{10}$ dopant/cm^2. These observations confirm that the antibody is specific to the SARS-CoV-2 spike protein. More experiments are required for testing other proteins and their mixtures and for statistical analysis of false positives and negatives. It is important to note that the most active sites for nonspecific binding can be the sites with unreacted PBASE on graphene. This is because PBASE has an *N*-hydroxysuccinimide ester group that can react covalently with amine groups in protein molecules. Therefore, in order to improve selectivity and specific binding, it will be important to cap these sites. In this work, we used amine-containing glycine to cap these unfunctionalized PBASE molecules (more information is provided in the Supporting Information).

To measure the sensor's sensitivity, we conducted experiments at several concentration ranges of the spike protein. Figure 4b and Table 1 show the change in the Fermi level of graphene when the device is interfaced with 1 pg/mL, 100 pg/mL, 10 ng/mL, 1 μg/mL, and 10 μg/mL SARS-CoV-2 spike protein in PBS. The results show an increase in graphene's 2D Raman shift with an increase in spike protein concentration. With the lowest concentration of 1 pg/mL (approximately 1.5 × 10^7 molecules/mL), there was a 0.83 cm^{-1} blue-shift. This Raman shift increased to 1.55, 1.98, 4.17, and 4.38 cm^{-1} with 100 pg/mL, 10 ng/mL, 1 μg/mL, and 10 μg/mL, respectively. Correspondingly, the Fermi level decreased from −313.9 meV

https://doi.org/10.1021/acsnano.1c02549
ACS Nano 2021, 15, 11743−11752

at 1 pg/mL to −337.3, −351.5, −434.9, and −445.6 meV at 100 pg/mL, 10 ng/mL, 1 μg/mL, and 10 μg/mL, respectively. The decreasing Fermi level of graphene with a higher concentration of CoV-2 S-protein reflects an increase of p-doping due to an increase in protein attachment. The asymptotic behavior of this response at higher spike protein concentration is attributed to the decreasing number of unoccupied surface antibody sites on this graphene transducer.

In addition, the detection at a lower concentration range (0.5 pg/mL, 1 pg/mL, 5 pg/mL, and 50 pg/mL) of CoV-2 spike protein in PBS also produced a similar trend (more information is provided in the Supporting Information). The lowest concentration tested for the spike protein in PBS was 1 fg/mL. Here, the 2D peak position increased from 2683.51 cm^{-1} to 2686.41 cm^{-1}, corresponding to a Fermi level change from −362.9 meV to −483.75 meV. The LOD[60] of this device in PBS is ∼1 fg/mL (more information is provided in the Supporting Information).

The LOD of our device with saliva as a base medium was also tested. The representative response of the graphene-PBASE-antibody device with low spike protein concentrations in saliva is shown in Figure 4b, inset (top, right). Here, the graphene's Fermi level decreases from −359.6 (blank sample) meV to −406.7, −465.4, −493.8, and −537.1 meV at 0.5, 1, 3, and 4 fg/mL, respectively. Accordingly, the 2D peak position increases from 2683.43 cm^{-1} (blank sample) to 2684.56, 2685.97, 2686.65, and 2687.69 cm^{-1}, respectively. The linear calibration curve for this response is Conc = (2D|pos − 2681.654)/0.878, and the standard deviation in the blank and 1 fg/mL data (using the highest observed standard deviation) gave a limit of blank (LOB) and LOD of 1.02 fg/mL and 3.75 fg/mL, respectively. The detailed calculation is provided in the Supporting Information (Section S5). These values are calculated from eight different locations, each location scanned with 3000 Raman spectra (3 s integration time with 1 ms acquisition time) and each spectrum containing 1024 wavenumbers (regression error is minimal in comparison to the standard deviation and is ignored (Section S9)).

It is important to emphasize that different devices can show different sensitivity. Since graphene, the base transducer in this device, is only one atom thick, it is inherently sensitive to its surroundings, especially the underlying substrate. More than 30 different devices have been tested, with all of them displaying the same direction of average change: an increase in 2D peak position with PBASE, a decrease in 2D peak position with antibody attachment, and an increase in 2D peak position with the attachment of COVID-19 spike protein (for concentrations above the LOD). Given this consistency, it is evident that the change is not coming from background/spectral noise. Further, it is important to note that the antibody molecules might not cover the entire area of the graphene surface with the same density. The percentage of graphene area that provides the response varies from 77% to 90%. Moreover, we need to ensure that the starting graphene sample is not heavily p-doped (generally, for a 2D position less than 2686 cm^{-1}); otherwise, the response becomes minimal. The CVD graphene used in this study had an average crystal size of 415 nm (measured by Raman;[61] see the Supporting Information). This implies that the Raman laser spot of 721 nm observes a few grain boundaries in our measurements. The sensor response can be further improved by using monocrystalline graphene with even better phononic sensitivity.

CONCLUSIONS

The high infection rate, long incubation period, and the possibility of asymptomatic infection necessitate the need for the development of rapid and sensitive detection techniques. In this work, we studied the phononic response of antibody-coupled graphene to CoV-2 spike protein as a foundation for a COVID-19 phononic sensor. Here, graphene functions as a Raman transducer, where its phononic properties are coupled with its interfacial properties, which are made selective to COVID-19 S-protein by chemically attaching COVID-19 antibody on graphene. The sensor showed no measurable cross-reactivity with MERS-CoV spike protein as well as other proteins in artificial human saliva. It was able to detect SARS-CoV-2 spike protein at the limit of detection of 1 fg/mL in PBS and 3.75 fg/mL in saliva. The graphene phononic sensor provides facile fabrication, potential for real-time response, and selective detection of target molecules. Importantly, with the versatility of this chemeo-phononic system, the surface chemistry can be modified to diagnose other viral variants and diseases.

MATERIALS AND METHODS

Graphene Growth. Graphene was grown on 25 μm thick copper foil (Alfa Aesar, 99.8%) using low-pressure chemical vapor deposition (LPCVD). Copper foils were immersed in $Fe(NO_3)_3/HNO_3$ solution (1 mol of $Fe(NO_3)_3$ and 3 mol of HNO_3) for 10 min of pretreatment to clean the copper oxide and impurities. After taking out from the $Fe(NO_3)_3/HNO_3$ solution, the copper foil was washed by acetone and isopropyl alcohol (IPA) and blow-dried with a N_2 gas. This clean Cu foil was then placed in a CVD furnace quartz tube, and the tube was allowed to reach a vacuum of <10 mTorr to reduce any further contamination in the system. After reaching low pressure, the CVD system was heated to 1050 °C from room temperature (25 °C) under 10 sccm H_2 in 25 min. At 1050 °C, the copper foil was annealed for a further 40 min with 10 sccm H_2 to prepare the copper foil surface for the deposition. The actual deposition occurs in the presence of precursor CH_4 at 10 sccm with a H_2 flow rate of 50 sccm. After 10 min of reaction, the CH_4 flow was removed to stop the supply of carbon source. H_2 flow was retained during the cool-down step of the process.

Transfer of Graphene. A Si/SiO_2 300 nm wafer chip was treated with piranha solution for 1 h, washed by DI water, acetone, and IPA, and blow-dried before the transfer. Graphene was transferred onto Si/SiO_2 300 nm using PMMA. PMMA powder was dissolved in anisole solvent at a concentration of 25 mg/mL. Then the PMMA solution was spin-coated onto graphene on the copper foil at 500 rpm in a 5 s ramping at 500 rpm/s, followed by 4000 rpm in a 30 s ramping at 1000 rpm/s. After that, the PMMA/graphene/copper foil was etched in HNO_3 98%/H_2O (1:3 by volume) for 1 h until all the copper was dissolved. The PMMA/graphene composite film that floated on the top was transferred to at least two DI water baths to remove the acid residues. The PMMA/graphene layer was then transferred onto a Si/SiO_2 chip and dried overnight. After that, the PMMA layer was removed by immersing the chip in acetone for 15 min. Then, the chip was washed by acetone and IPA and dried with blowing N_2. Finally, the chip was annealed at high temperature and low pressure to further reduce polymer and other sources of contamination.

Functionalization of Graphene with PBASE. PBASE powder was stored in a freezer (−5 to −30 °C) and protected from light. Graphene on a Si/SiO_2 wafer was immersed in 2 mM PBASE in methanol for 1 h at room temperature. Afterward, the PBASE-modified graphene was washed with methanol and dried with N_2.

Immobilization of SARS-CoV-2 Spike Antibody on the Graphene Surface. A 10 μL amount of SARS-CoV-2 spike antibody of 250 μg/mL in PBS (pH = 7.4) solvent was dropped on graphene-PBASE. The immobilization reaction lasted for 4 h at 4 °C. The chip was then rinsed with PBS and DI water and dried with N_2. The

https://doi.org/10.1021/acsnano.1c02549
ACS Nano 2021, 15, 11743−11752

activity of antibodies does not show a detectable loss up to one month when kept at 2−8 °C; therefore, for storage purposes, the final antibody-graphene device must be stored in PBS buffer at 2−8 °C.

Capping Unreacted PBASE with Glycine to Reduce Spike Protein Nonspecific Binding. The graphene-PBASE-antibody structure was immersed in glycine solution (0.2 g of glycine in 10 mL of PBS, pH = 7.4) for 30 min. After that, the device was rinsed with DI water three times and dried with N_2.

Immobilization of SARS-CoV-2 Spike Protein and MERS-CoV Protein on the Graphene Surface. SARS-CoV-2 and MERS-CoV spike proteins in PBS (pH = 7.4) solvent at different concentrations were dropped on the graphene-PBASE-antibody structure. The reactions lasted for 30 min at 4 °C. After that, the chip was rinsed with PBS and DI water and dried with N_2.

ASSOCIATED CONTENT

Supporting Information

The Supporting Information is available free of charge at https://pubs.acs.org/doi/10.1021/acsnano.1c02549.

> Amino acid sequences, Raman liquid scan for the 2D band in PBS buffer, spike protein detection in PBS at low concentration, limit of detection of SARS-CoV-2 spike protein in PBS, limit of detection of SARS-CoV-2 spike protein in artificial saliva, comparison between our work and other detection techniques, reduction of spike protein nonspecific binding by capping unreacted PBASE with glycine, voltage calculation, regression error, graphene grain size estimation, and XPS analysis of the antibody attachment (PDF)

AUTHOR INFORMATION

Corresponding Author

Vikas Berry − *Department of Chemical Engineering, University of Illinois at Chicago, Chicago, Illinois 60607, United States;* orcid.org/0000-0002-1102-1996; Email: vikasb@uic.edu

Authors

Ngoc Hoang Lan Nguyen − *Department of Chemical Engineering, University of Illinois at Chicago, Chicago, Illinois 60607, United States*

Sungjoon Kim − *Department of Chemical Engineering, University of Illinois at Chicago, Chicago, Illinois 60607, United States*

Garrett Lindemann − *Ramaco LLC, Sheridan, Wyoming 82801, United States*

Complete contact information is available at: https://pubs.acs.org/10.1021/acsnano.1c02549

Notes

The authors declare the following competing financial interest(s): A provisional patent has been applied for based on this work.

ACKNOWLEDGMENTS

V.B. acknowledges financial support from Ramaco Carbon, Office of Naval Research (N00014-18-1-2583), and University of Illinois at Chicago. The authors acknowledge support from Research Resources Center at UIC for the use of XPS. The authors thank A. Mehta, B. Keisham, S. Behura, and R. Nemade for important discussions.

REFERENCES

(1) Zhu, N.; Zhang, D.; Wang, W.; Li, X.; Yang, B.; Song, J.; Zhao, X.; Huang, B.; Shi, W.; Lu, R.; Niu, P.; Zhan, F.; Ma, X.; Wang, D.; Xu, W.; Wu, G.; Gao, G. F.; Tan, W. A Novel Coronavirus from Patients with Pneumonia in China, 2019. *N. Engl. J. Med.* **2020**, *382*, 727.

(2) Guan, W.; Ni, Z.; Hu, Y.; Liang, W.; Ou, C.; He, J.; Liu, L.; Shan, H.; Lei, C.; Hui, D. S. C.; Du, B.; Li, L.; Zeng, G.; Yuen, K.-Y.; Chen, R.; Tang, C.; Wang, T.; Chen, P.; Xiang, J.; Li, S.; et al. Clinical Characteristics of Coronavirus Disease 2019 in China. *N. Engl. J. Med.* **2020**, *382*, 1708.

(3) Johns Hopkins Coronavirus Resource Center. https://coronavirus.jhu.edu/map.html (accessed May 29, 2021).

(4) Li, F. Structure, Function, and Evolution of Coronavirus Spike Proteins. *Annu. Rev. Virol.*. **2016**, *3*, 237.

(5) Li, W.; Moore, M. J.; Vasllieva, N.; Sui, J.; Wong, S. K.; Berne, M. A.; Somasundaran, M.; Sullivan, J. L.; Luzuriaga, K.; Greeneugh, T. C.; Choe, H.; Farzan, M. Angiotensin-Converting Enzyme 2 Is a Functional Receptor for the SARS Coronavirus. *Nature* **2003**, *426*, 450.

(6) Xu, J.; Wu, R.; Huang, H.; Zheng, W.; Ren, X.; Wu, N.; Ji, B.; Lv, Y.; Liu, Y.; Mi, R. Computed Tomographic Imaging of 3 Patients with Coronavirus Disease 2019 Pneumonia with Negative Virus Real-Time Reverse-Transcription Polymerase Chain Reaction Test. *Clin. Infect. Dis.* **2020**, *71*, 850.

(7) Corman, V. M.; Eckerle, I.; Bleicker, T.; Zaki, A.; Landt, O.; Eschbach-Bludau, M.; van Boheemen, S.; Gopal, R.; Ballhause, M.; Bestebroer, T. M.; Muth, D.; Müller, M. A.; Drexler, J. F.; Zambon, M.; Osterhaus, A. D.; Fouchier, R. M.; Drosten, C. Detection of a Novel Human Coronavirus by Real-Time Reverse-Transcription Polymerase Chain Reaction. *Eurosurveillance* **2012**, *17*, 1−6.

(8) Xie, X.; Zhong, Z.; Zhao, W.; Zheng, C.; Wang, F.; Liu, J. Chest CT for Typical Coronavirus Disease 2019 (COVID-19) Pneumonia: Relationship to Negative RT-PCR Testing. *Radiology* **2020**, *296*, E41.

(9) Seo, G.; Lee, G.; Kim, M. J.; Baek, S.-H.; Choi, M.; Ku, K. B.; Lee, C.-S.; Jun, S.; Park, D.; Kim, H. G.; Kim, S.-J.; Lee, J.-O.; Kim, B. T.; Park, E. C.; Kim, S. Il. Rapid Detection of COVID-19 Causative Virus (SARS-CoV-2) in Human Nasopharyngeal Swab Specimens Using Field-Effect Transistor-Based Biosensor. *ACS Nano* **2020**,*14*, 5135.

(10) Kim, S.; Keisham, B.; Berry, V. Cellular Nano-Transistor: An Electronic-Interface between Nanoscale Semiconductors and Biological Cells. *Mater. Today Nano* **2020**, *9*, 100063.

(11) Qiu, G.; Gai, Z.; Tao, Y.; Schmitt, J.; Kullak-Ublick, G. A.; Wang, J. Dual-Functional Plasmonic Photothermal Biosensors for Highly Accurate Severe Acute Respiratory Syndrome Coronavirus 2 Detection. *ACS Nano* **2020**, *14*, 5268−5277.

(12) Moitra, P.; Alafeef, M.; Alafeef, M.; Alafeef, M.; Dighe, K.; Frieman, M. B.; Pan, D.; Pan, D.; Pan, D. Selective Naked-Eye Detection of SARS-CoV-2 Mediated by N Gene Targeted Antisense Oligonucleotide Capped Plasmonic Nanoparticles. *ACS Nano* **2020**, *14*, 7617−7627.

(13) Cai, X. F.; Chen, J.; Hu, J. li; Long, Q. X.; Deng, H. J.; Liu, P.; Fan, K.; Liao, P.; Liu, B. Z.; Wu, G. C.; Chen, Y. K.; Li, Z. J.; Wang, K.; Zhang, X. L.; Tian, W. G.; Xiang, J. L.; Du, H. X.; Wang, J.; Hu, Y.; Tang, N.; et al. A Peptide-Based Magnetic Chemiluminescence Enzyme Immunoassay for Serological Diagnosis of Coronavirus Disease 2019. *J. Infect. Dis.* **2020**, *222*, 189−195.

(14) Infantino, M.; Grossi, V.; Lari, B.; Bambi, R.; Perri, A.; Manneschi, M.; Terenzi, G.; Liotti, I.; Ciotta, G.; Taddei, C.; Benucci, M.; Casprini, P.; Veneziani, F.; Fabbri, S.; Pompetti, A.; Manfredi, M. Diagnostic Accuracy of an Automated Chemiluminescent Immunoassay for Anti-SARS-CoV-2 IgM and IgG Antibodies: An Italian Experience. *J. Med. Virol.* **2020**, *92*, 1671−1675.

(15) Wan, Y.; Shang, J.; Graham, R.; Baric, R. S.; Li, F. Receptor Recognition by the Novel Coronavirus from Wuhan: An Analysis Based on Decade-Long Structural Studies of SARS Coronavirus. *J. Virol.* **2020**, *94*, 1−9.

(16) Carter, L. J.; Garner, L. V.; Smoot, J. W.; Li, Y.; Zhou, Q.; Saveson, C. J.; Sasso, J. M.; Gregg, A. C.; Soares, D. J.; Beskid, T. R.; Jervey, S. R.; Liu, C. Assay Techniques and Test Development for COVID-19 Diagnosis. *ACS Cent. Sci.* **2020**, *6*, 591−605.
(17) Basko, D. M.; Piscanec, S.; Ferrari, A. C. Electron-Electron Interactions and Doping Dependence of the Two-Phonon Raman Intensity in Graphene. *Phys. Rev. B: Condens. Matter Mater. Phys.* **2009**, *80*, 1−10.
(18) Ahmadian Yazdi, A.; Xu, J.; Berry, V. Phononics of Graphene Interfaced with Flowing Ionic Fluid: An Avenue for High Spatial Resolution Flow Sensor Applications. *ACS Nano* **2021**,*15*, 6998.
(19) Das, A.; Pisana, S.; Chakraborty, B.; Piscanec, S.; Saha, S. K.; Waghmare, U. V.; Novoselov, K. S.; Krishnamurthy, H. R.; Geim, A. K.; Ferrari, A. C.; Sood, A. K. Monitoring Dopants by Raman Scattering in an Electrochemically Top-Gated Graphene Transistor. *Nat. Nanotechnol.* **2008**, *3*, 210−215.
(20) Ferrari, A. C.; Meyer, J. C.; Scardaci, V.; Casiraghi, C.; Lazzeri, M.; Mauri, F.; Piscanec, S.; Jiang, D.; Novoselov, K. S.; Roth, S.; Geim, A. K. Raman Spectrum of Graphene and Graphene Layers. *Phys. Rev. Lett.* **2006**, *97*, 1−4.
(21) Malard, L. M.; Pimenta, M. A.; Dresselhaus, G.; Dresselhaus, M. S. Raman Spectroscopy in Graphene. *Phys. Rep.* **2009**, *473*, 51−87.
(22) Ferrari, A. C. Raman Spectroscopy of Graphene and Graphite: Disorder, Electron-Phonon Coupling, Doping and Nonadiabatic Effects. *Solid State Commun.* **2007**, *143*, 47−57.
(23) Ferrari, A. C.; Basko, D. M. Raman Spectroscopy as a Versatile Tool for Studying the Properties of Graphene. *Nat. Nanotechnol.* **2013**, *8*, 235−246.
(24) Lazzeri, M.; Mauri, F. Nonadiabatic Kohn Anomaly in a Doped Graphene Monolayer. *Phys. Rev. Lett.* **2006**, *97*, 29−32.
(25) Pisana, S.; Lazzeri, M.; Casiraghi, C.; Novoselov, K. S.; Geim, A. K.; Ferrari, A. C.; Mauri, F. Breakdown of the Adiabatic Born-Oppenheimer Approximation in Graphene. *Nat. Mater.* **2007**, *6*, 198−201.
(26) Casiraghi, C. Doping Dependence of the Raman Peaks Intensity of Graphene Close to the Dirac Point. *Phys. Rev. B: Condens. Matter Mater. Phys.* **2009**, *80*, 2−4.
(27) Keisham, B.; Cole, A.; Nguyen, P.; Mehta, A.; Berry, V. Cancer Cell Hyperactivity and Membrane Dipolarity Monitoring via Raman Mapping of Interfaced Graphene: Toward Non-Invasive Cancer Diagnostics. *ACS Appl. Mater. Interfaces* **2016**, *8*, 32717−32722.
(28) Keisham, B.; Seksenyan, A.; Denyer, S.; Kheirkhah, P.; Arnone, G. D.; Avalos, P.; Bhimani, A. D.; Svendsen, C.; Berry, V.; Mehta, A. I. Quantum Capacitance Based Amplified Graphene Phononics for Studying Neurodegenerative Diseases. *ACS Appl. Mater. Interfaces* **2019**, *11*, 169−175.
(29) Butler, H. J.; Ashton, L.; Bird, B.; Cinque, G.; Curtis, K.; Dorney, J.; Esmonde-White, K.; Fullwood, N. J.; Gardner, B.; Martin-Hirsch, P. L.; Walsh, M. J.; McAinsh, M. R.; Stone, N.; Martin, F. L. Using Raman Spectroscopy to Characterize Biological Materials. *Nat. Protoc.* **2016**, *11*, 664−687.
(30) Gremlich, H.-U.; Yan, B. *Infrared and Raman Spectroscopy of Biological Materials*; CRC Press: New York, 2000.
(31) Pinto, H.; Markevich, A. Electronic and Electrochemical Doping of Graphene by Surface Adsorbates. *Beilstein J. Nanotechnol.* **2014**, *5*, 1842−1848.
(32) Li, Y. *Probing the Response of Two-Dimensional Crystals by Optical Spectroscopy*; Ph.D. Thesis, 2016; pp 45−54.
(33) Li, X.; Cai, W.; An, J.; Kim, S.; Nah, J.; Yang, D.; Piner, R.; Velamakanni, A.; Jung, I.; Tutuc, E.; Banerjee, S. K.; Colombo, L.; Ruoff, R. S. Large-Area Synthesis of High-Quality and Uniform Graphene Films on Copper Foils. *Science (Washington, DC, U. S.)* **2009**, *324*, 1312−1314.
(34) Goniszewski, S.; Adabi, M.; Shaforost, O.; Hanham, S. M.; Hao, L.; Klein, N. Correlation of P-Doping in CVD Graphene with Substrate Surface Charges. *Sci. Rep.* **2016**, *6*, 1−9.
(35) Wu, G.; Tang, X.; Meyyappan, M.; Lai, K. W. C. Doping Effects of Surface Functionalization on Graphene with Aromatic Molecule and Organic Solvents. *Appl. Surf. Sci.* **2017**, *425*, 713−721.
(36) Wang, Y.; Chen, X.; Zhong, Y.; Zhu, F.; Loh, K. P. Large Area, Continuous, Few-Layered Graphene as Anodes in Organic Photovoltaic Devices. *Appl. Phys. Lett.* **2009**, *95*, 1−4.
(37) Wang, S.; Hossain, Z.; Shinozuka, K.; Shimizu, N.; Kitada, S. *Graphene Field-Effect Transistor Biosensor for Detection of Biotin with Ultrahigh Sensitivity and Specificity*. 2020, No. January.
(38) Kwong Hong Tsang, D.; Lieberthal, T. J.; Watts, C.; Dunlop, I. E.; Ramadan, S.; del Rio Hernandez, A. E.; Klein, N. Chemically Functionalised Graphene FET Biosensor for the Label-Free Sensing of Exosomes. *Sci. Rep.* **2019**, *9*, DOI: 10.1038/s41598-019-50412-9.
(39) Ripalda, J. M.; Montero, I.; Galán, L. An XPS Study of Carbon Nitride Synthesized by Ion Beam Nitridation of C60 Fullerene. *Diamond Relat. Mater.* **1998**, *7*, 402−406.
(40) Torabizadeh, H. All Proteins Have a Basic Molecular Formula. *World Acad. Sci. Eng. Technol.* **2011**, *78*, 961−965.
(41) Calizo, I.; Balandin, A. A.; Bao, W.; Miao, F.; Lau, C. N. Temperature Dependence of the Raman Spectra of Graphene and Graphene Multilayers. *Nano Lett.* **2007**, *7*, 2645−2649.
(42) Calizo, I.; Miao, F.; Bao, W.; Lau, C. N.; Balandin, A. A. Variable Temperature Raman Microscopy as a Nanometrology Tool for Graphene Layers and Graphene-Based Devices. *Appl. Phys. Lett.* **2007**, *91*, 071913.
(43) Deng, S.; Rhee, D.; Lee, W. K.; Che, S.; Keisham, B.; Berry, V.; Odom, T. W. Graphene Wrinkles Enable Spatially Defined Chemistry. *Nano Lett.* **2019**, *19*, 5640−5646.
(44) Ni, Z. H.; Yu, T.; Lu, Y. H.; Wang, Y. Y.; Feng, Y. P.; Shen, Z. X. Uniaxial Strain on Graphene: Raman Spectroscopy Study and Band-Gap Opening. *ACS Nano* **2008**, *2*, 2301−2305.
(45) Larsen, M. B. B. S.; Mackenzie, D. M. A.; Caridad, J. M.; Bøggild, P.; Booth, T. J. Transfer Induced Compressive Strain in Graphene: Evidence from Raman Spectroscopic Mapping. *Microelectron. Eng.* **2014**, *121*, 113−117.
(46) Lee, J. E.; Ahn, G.; Shim, J.; Lee, Y. S.; Ryu, S. Optical Separation of Mechanical Strain from Charge Doping in Graphene. *Nat. Commun.* **2012**, *3*, DOI: 10.1038/ncomms2022.
(47) Mueller, N. S.; Heeg, S.; Alvarez, M. P.; Kusch, P.; Wasserroth, S.; Clark, N.; Schedin, F.; Parthenios, J.; Papagelis, K.; Galiotis, C.; Kalbáč, M.; Vijayaraghavan, A.; Huebner, U.; Gorbachev, R.; Frank, O.; Reich, S. Evaluating Arbitrary Strain Configurations and Doping in Graphene with Raman Spectroscopy. *2D Mater.* **2018**, *5*, 015016.
(48) Huang, M.; Yan, H.; Heinz, T. F.; Hone, J. Probing Strain-Induced Electronic Structure Change in Graphene by Raman Spectroscopy. *Nano Lett.* **2010**, *10*, 4074−4079.
(49) Froehlicher, G.; Berciaud, S. Raman Spectroscopy of Electrochemically Gated Graphene Transistors: Geometrical Capacitance, Electron-Phonon, Electron-Electron, and Electron-Defect Scattering. *Phys. Rev. B: Condens. Matter Mater. Phys.* **2015**, DOI: 10.1103/PhysRevB.91.205413.
(50) Wang, Y. Y.; Ni, Z. H.; Yu, T.; Shen, Z. X.; Wang, H. M.; Wu, Y. H.; Chen, W.; Wee, A. T. S. Raman Studies of Monolayer Graphene: The Substrate Effect. *J. Phys. Chem. C* **2008**, *112*, 10637−10640.
(51) Calizo, I.; Bao, W.; Miao, F.; Lau, C. N.; Balandin, A. A. The Effect of Substrates on the Raman Spectrum of Graphene: Graphene-on-Sapphire and Graphene-on-Glass. *Appl. Phys. Lett.* **2007**, *91*, 1−4.
(52) Woehrl, N.; Ochedowski, O.; Gottlieb, S.; Shibasaki, K.; Schulz, S. Plasma-Enhanced Chemical Vapor Deposition of Graphene on Copper Substrates. *AIP Adv.*. **2014**, *4*, 047128.
(53) Kumar, A.; White, J.; James Christie, R.; Dimasi, N.; Gao, C. Antibody-Drug Conjugates. *Platform Technologies in Drug Discovery and Validation*, 1st ed.; Elsevier: Annual Reports in Medicinal Chemistry; 2017; Vol. *50*, pp 441−480.
(54) Al-Owaedi, O. A.; Khalil, T. T.; Karim, S. A.; Said, M. H.; Al-Bermany, E.; Taha, D. N. The Promising Barrier: Theoretical Investigation. *Syst. Rev. Pharm.* **2020**, *11*, 110−115.
(55) Adhikari, P.; Li, N.; Shin, M.; Steinmetz, N. F.; Twarock, R.; Podgornik, R.; Ching, W. Y. Intra- And Intermolecular Atomic-Scale Interactions in the Receptor Binding Domain of SARS-CoV-2 Spike

Protein: Implication for ACE2 Receptor Binding. *Phys. Chem. Chem. Phys.* **2020**, *22*, 18272−18283.
(56) Docter, D.; Bantz, C.; Westmeier, D.; Galla, H. J.; Wang, Q.; Kirkpatrick, J. C.; Nielsen, P.; Maskos, M.; Stauber, R. H. The Protein Corona Protects against Size- and Dose-Dependent Toxicity of Amorphous Silica Nanoparticles. *Beilstein J. Nanotechnol.* **2014**, *5*, 1380−1392.
(57) Xia, J.; Chen, F.; Li, J.; Tao, N. Measurement of the Quantum Capacitance of Graphene. *Nat. Nanotechnol.* **2009**, *4*, 505−509.
(58) Kim, C. H.; Frisbie, C. D. Determination of Quantum Capacitance and Band Filling Potential in Graphene Transistors with Dual Electrochemical and Field-Effect Gates. *J. Phys. Chem. C* **2014**, *118*, 21160−21169.
(59) Ke, Z.; Oton, J.; Qu, K.; Cortese, M.; Zila, V.; McKeane, L.; Nakane, T.; Zivanov, J.; Neufeldt, C. J.; Cerikan, B.; Lu, J. M.; Peukes, J.; Xiong, X.; Kräusslich, H. G.; Scheres, S. H. W.; Bartenschlager, R.; Briggs, J. A. G. Structures and Distributions of SARS-CoV-2 Spike Proteins on Intact Virions. *Nature* **2020**, *588*, 498−502.
(60) Armbruster, D. A.; Pry, T. Limit of Blank, Limit of Detection and Limit of Quantitation. *Clin. Biochem. Rev.* **2008**, *29*, S49−52.
(61) Ribeiro-Soares, J.; Oliveros, M. E.; Garin, C.; David, M. V.; Martins, L. G. P.; Almeida, C. A.; Martins-Ferreira, E. H.; Takai, K.; Enoki, T.; Magalhães-Paniago, R.; Malachias, A.; Jorio, A.; Archanjo, B. S.; Achete, C. A.; Cançado, L. G. Structural Analysis of Polycrystalline Graphene Systems by Raman Spectroscopy. *Carbon* **2015**, *95*, 646−652.

https://doi.org/10.1021/acsnano.1c02549
ACS Nano 2021, 15, 11743−11752